

---

## Asymptotic Solutions of Algebraic Reynolds Stress Model Applied to Rough Bottom Open Channel Flow

Amel Soualmia<sup>a\*</sup>, Sahbi Zaouali<sup>b</sup>, Lucien Masbernat<sup>c</sup>

<sup>a</sup> *Laboratoire Science et Technologie de l'eau de l'INAT, 43 Avenue Charles Nicolle, 1082 Tunis, Tunisie*

<sup>b</sup> *Ecole Nationale d'Ingénieurs de Tunis, laboratoire (LMHE), BP 37 Le Belvédère, 1002 Tunis, Tunisie*

<sup>c</sup> *Institut de Mécanique des Fluides de Toulouse, Allée du Prof. Camille Soula, 31400 Toulouse, France*

<sup>a</sup> *Email: amel.inat@hotmail.fr*

<sup>b</sup> *Email: sahbi.zaouali@enit.rnu.tn*

<sup>c</sup> *Email: Lucien.Masbernat@imft.fr*

### Abstract

We interpret experimental results on the structure of an open channel flow with a strong transverse variation of the bottom roughness. Knowing the wall parameters, we analyze the behavior of Reynolds stress components by using asymptotic solutions of an algebraic stress model developed in the wall and free surface regions. This analysis allowed us to emphasize effects of secondary flows on the production of turbulence near the wall, and the capability of this model to predict the normal components of the Reynolds tensor in the wall and free surface regions when the turbulent shear stresses are well predicted.

**Keywords:** Open channel; rib rough bed; Secondary flows; Turbulent flow; Anisotropy; algebraic stress model.

### 1. Introduction

In open channel flows, with bottom roughness heterogeneity, the turbulence anisotropy, amplified by wall and free surface interactions, drives secondary motions that alter significantly the structure of the flow. The prediction of such flows requires second-order closure models that should be able to reproduce adequately the anisotropy of the Reynolds stresses. Despite the progress in turbulence modeling during the past three decades [1, 2, 3], some recurrent questions yet remain to predict free surface flows with complex wall roughness configurations as this is the case in most natural flows. In such flows, the presence of a cross-stream variation in the bottom roughness accompanied by secondary flows, introduces specific interactions between the mean flow and the turbulence, in the whole flow field.

---

\* Corresponding author.

E-mail address: amel.inat@hotmail.fr.

Moreover, in fully developed flows, turbulent shear stress and mean velocity profiles are strongly affected by the momentum transport by the secondary flows that have certainly an important effect on the turbulence production in the wall zone [4, 5, 6, 7]. Some recent experimental works [8, 9, 10, 11, 12] confirmed these effects, Although these experiments yield contour maps of mean velocity and turbulent stresses without a detailed analysis of Reynolds stresses behaviors, in the wall and free surface zones. However, further experiments on reference roughness configuration are essential to analyze the performances and the limits of turbulence models. In this paper, results of an experience [13, 14] achieved in a free surface flows above non-homogeneous rough bottom in a rectangular channel were used.

Within the framework of this study, to analyze the evolution of Reynolds stresses profiles, we had developed an asymptotic formulation of a Reynolds stress model adapted to the free surface flows by [1]. This solution is based on two assumptions: in the wall region we consider the equilibrium production-dissipation, and near the free surface we consider that the production of turbulence decreases, and the turbulent kinetic energy is mainly controlled by the transport and the local dissipation.

## 2. Asymptotic solutions of algebraic Reynolds stress model near the wall and the free surface

In the following, we note that  $x$  and  $y$  are the longitudinal and transverse coordinates,  $z$  is the coordinate normal to the channel bed ;  $U, V, W$  and  $u, v, w$ , are the  $(x, y, z)$ -components of the mean velocity and velocity fluctuations, respectively. At first, we expressed the turbulent stress tensor components by the algebraic expressions issued from the Reynolds-stress transport model of [15] adapted by [1] to simulate wall and free surface effects on the partition of the turbulent energy in open channel flows. Neglecting lateral wall effects and with the assumption of a fully developed turbulent flow, the normal components of the Reynolds tensor can be written as:

$$\frac{\overline{u^2}}{k} = \frac{2}{3(C_1 + \widehat{P}_r - 1)} [C_1 - 1 + (3 - 2C_2 + C_2 c'_2 f) \widehat{P}_r + c'_1 f \frac{\overline{w^2}}{k}] \tag{1}$$

$$\frac{\overline{v^2}}{k} = \frac{2}{3(C_1 + \widehat{P}_r - 1)} [C_1 - 1 + C_2(1 + c'_2 f) \widehat{P}_r + \frac{3}{2} c'_1 f \frac{\overline{w^2}}{k}] \tag{2}$$

$$\frac{\overline{w^2}}{k} = \frac{2}{3} \frac{C_1 - 1 + C_2(1 - 2c'_2 f) \widehat{P}_r}{C_1 + \widehat{P}_r - 1 + 2c'_1 f} \tag{3}$$

The turbulent shear stresses may be expressed as follow:

$$-\overline{uw} = C_{\mu z} \frac{k^2}{\varepsilon} \frac{\partial U}{\partial z} \quad \text{with} \quad C_{\mu z} = A \frac{1 - C_2 + \frac{3}{2} C_2 c'_2 f}{C_1 - 1 + \widehat{P}_r + \frac{3}{2} c'_1 f} \frac{\overline{w^2}}{k} \tag{4}$$

$$-\overline{uv} = C_{\mu y} \frac{k^2}{\varepsilon} \frac{\partial U}{\partial y} \quad \text{with} \quad C_{\mu y} = A \frac{(1 - C_2)}{(C_1 - 1 + \widehat{P}_r)} \frac{\overline{v^2}}{k} \tag{5}$$

In these equations,  $\widehat{P}_r = P_r / \varepsilon$  is the ratio between the production rate  $P_r$  and the dissipation rate  $\varepsilon$  of the turbulent kinetic energy  $k$  ;  $C_{\mu y}$  and  $C_{\mu z}$  are the turbulent viscosity coefficients and the surface-proximity function  $f$  accounts for the damping of the vertical velocity component by the wall and the free surface. [1] proposed to

express  $f$ , according to the depth flow  $h$  and the dimensionless height  $\xi = z/h$ , as:

$$f = \frac{L}{ah} \left[ \underbrace{\xi^{-1}(1-\xi)^2}_{\text{Wall effect}} + \underbrace{\xi^2(1-\xi)^{-1}}_{\text{Free surface effect}} \right] \quad (6)$$

In Eq.(6),  $L$  is a characteristic length scale of energy containing eddies defined as:  $L = k^{3/2} / \varepsilon$  (7)

The standard values of the constants in the model of [14] are  $[C_1, C_2, c_1, c_2] = [1.8, 0.6, 0.5, 0.3]$  and the constant  $A = 1$  in the expressions (4) and (5). In the present work we'll take  $A < 1$ , because  $A = 1$  gives too high values of  $C_{\mu z}$  and, consequently, too small values of turbulence intensity in the wall region. In the expression (6) of the surface proximity function, the constant  $a$  of adjustment of the length scale  $L$  is expressed by:

$$a = \kappa C_{\mu w}^{-3/4} (1 - \xi_w)^{2.5} \quad (8)$$

As for the value  $a = 3.18$ , fixed by [1], the simulation by equation (8) leads to the standard values  $\overline{w^2} / k \approx 0.25$  and  $\overline{u^2} / k \approx 1.1$  very close to the wall ( $\xi_w = 0.05$  for which  $C_{\mu z} = C_{\mu w}$ ), when  $f = 1$ .

### 2.1. The wall region of production-dissipation equilibrium

The local equilibrium assumption yields  $\widehat{P}_r = 1$ . If we neglect the turbulence production by the secondary motions, the production rate and the dissipation rate in the equilibrium zone may be written as:

$$P_r = \varepsilon = -\overline{uw} \frac{\partial U}{\partial z} - \overline{uv} \frac{\partial U}{\partial y} = -\overline{uw} \frac{\partial U}{\partial z} (1 + R_p) \quad (9)$$

Where the production ratio  $R_p$  is defined as  $R_p = (-\overline{uv} \frac{\partial U}{\partial y}) / (-\overline{uw} \frac{\partial U}{\partial z})$ .

From equations (4) and (5), the production ratio may be expressed as:  $R_p = \frac{C_{\mu y}}{C_{\mu z}} R_S$  (10)

The shearing ratio  $R_S$  is defined as:  $R_S = (\frac{\partial U}{\partial y} / \frac{\partial U}{\partial z})^2$  (11)

On the other hand, in the equilibrium region, the logarithmic law is verified and:  $\frac{\partial U}{\partial z} = (\kappa z)^{-1}$  (12)

Hence, with equations (9) and (12), the non-dimensional dissipation rate may be written as:

$$\varepsilon^+ = \frac{\varepsilon h}{u_*^3} = (1 + \frac{C_{\mu y}}{C_{\mu z}} R_S) (\frac{-\overline{uw}}{u_*^2}) (\kappa \xi)^{-1} \quad (13)$$

From equations (4) and (12), we obtain the dimensionless turbulent kinetic energy as:

$$k^+ = \frac{k}{u_*^2} = [C_{\mu z}^{-1} (1 + \frac{C_{\mu y}}{C_{\mu z}} R_S)]^{0.5} (\frac{-\overline{uw}}{u_*^2}) \quad (14)$$

Finally, equations (13) and (14) give the expression of the length scale  $L$  defined by (7):

$$L^+ = L/h = \kappa C_{\mu\epsilon}^{-3/4} \left(1 + \frac{C_{\mu y}}{C_{\mu\epsilon}} R_S\right)^{-0.25} \left(\frac{-\overline{uw}}{u^{*2}}\right)^{0.5} \xi \tag{15}$$

We note that the asymptotic solutions of  $P_r$ ,  $k$  and  $L$  in the wall region and near the free surface are a function of the turbulent shear stress. To reproduce the experimental results of [13, 14] we use, in the outer region, the smoothing of the measured profiles of  $-\overline{uw}/u^{*2}$  which reflect the effect of the secondary flow on the transport of the longitudinal momentum (see continuous lines on fig.5). Very close to the wall, where there is no measurement, the dimensionless shear stress  $-\overline{uw}/u^{*2}$  will be calculated by:

$$-\overline{uw}/u^{*2} = 1 - \alpha\xi \tag{16}$$

Values  $\alpha$  may be also associated to the transport of longitudinal momentum by the secondary flows and represent a decrease or the increase of turbulence production in the wall region (see fig.5).

To determine the production ratio  $R_p$  given by (10), we expressed the shearing ratio  $R_S$  from the logarithmic law ( $U^+ = U/u^* = \kappa^{-1} \ln(Z^+) + C(K_S^+)$  with  $Z^+ = u^*Z/\nu$  and  $Z = z + z_0$ ) as a function of the transverse gradient of the friction velocity  $u^*$  and the roughness function  $C$  in the form:

$$R_S = \kappa^2 \left(\frac{h}{B}\right)^2 \left[ \left( U^+ + \frac{1}{\kappa} \right) \frac{1}{u^*} \frac{\partial u^*}{\partial \zeta} + \frac{\partial C}{\partial \zeta} \right]^2 \xi^2 \tag{17}$$

In Eq.(17),  $B$  is the half channel width and  $\zeta$  is dimensionless width ( $\zeta = y/B$ ). The gradients of the friction velocity and the roughness function above the channel bottom was calculated from the smoothing of experimental results (Run Za) [13] presented in fig. 1.

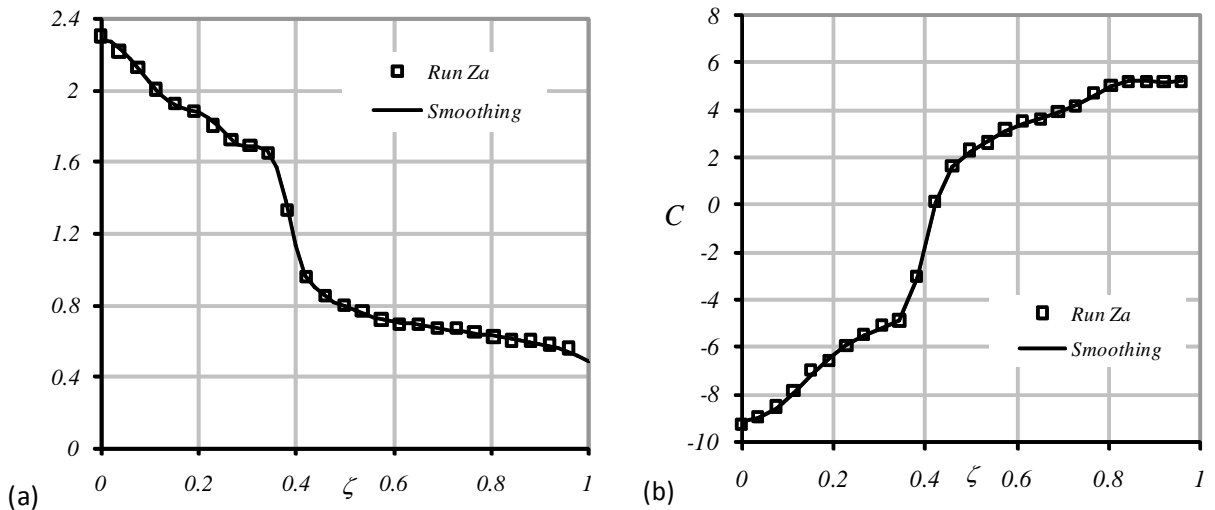


Fig. 1. Transversal distributions of: (a) the bottom friction; (b) the roughness function  $C$

The previous equations allow to calculate the Reynolds stress components  $\overline{u^2}/u^{*2}$  and  $\overline{w^2}/u^{*2}$  versus  $\xi$  by means of an iteration on the values of the turbulent viscosity coefficients  $C_{\mu\epsilon}$  and  $C_{\mu y}$  given by Eq. (4) and (5).

Indeed, with given values of  $C_{\mu z}$  and  $C_{\mu y}$ , Eq.(14), (15), (16) and (17) allow calculation of the kinetic energy and the turbulent scale and consequently the surface proximity function  $f$  by Eq.(6). We can then calculate the Reynolds stress components  $\overline{u^2}/k$  and  $\overline{w^2}/k$  given by Eq.(1) and (3) and the new values of  $C_{\mu z}$  and  $C_{\mu y}$  and so on.

### 2.2. The free surface region of weak turbulence production

Near the free surface, the production of turbulence decreases and the turbulent kinetic energy is mainly controlled by the transport and the local dissipation. If we assume the flow is fully developed and parallel, the equation of turbulent kinetic energy takes the form:

$$\frac{\partial}{\partial z} \left( \frac{C_{\mu z} k^2}{\sigma_k \varepsilon} \frac{\partial k}{\partial z} \right) + \frac{\varepsilon}{C_{\mu z} k^2} (\overline{-uw})^2 - \varepsilon = 0 \tag{18}$$

The effect of the secondary flows on the transport of the longitudinal momentum, at the free surface region, is taken into account by considering a linear approximation of the profile of the turbulent shear stress, expressed in the form:

$$(\overline{-uw}) = \sqrt{\gamma} u^{*2} (1 - \xi) \tag{19}$$

The constant  $\gamma$  is determined from the experimental profiles of the turbulent shear stress, as presented in fig.5. This hypothesis is completely acceptable for vertical profiles between  $y=0$  to  $y=16$ .

We developed an analytical solution of (18) by assuming a constant value of the length scale  $L = k^{3/2} / \varepsilon$ , as a well-known consequence of the equilibrium between diffusion and dissipation. So, we put:

$$L = L_s = \text{Constant} \quad \text{and} \quad \varepsilon = k^{3/2} / L_s \tag{20}$$

where "s" index indicates values of the different quantities at the free surface  $\xi = 1$ .

In the model of [15], the coefficient  $C_{\mu z}$  and the turbulent Prandtl number  $\sigma_k$  are not constant:  $C_{\mu z}$  is given by Eq. (4) and  $\sigma_k$  is expressed as:

$$\sigma_k = c_k^{-1} (C_1 - 1 + \hat{P}_r + \frac{3}{2} c_1' f)^{-1} (1 - C_2 + \frac{3}{2} C_2 c_2' f) \tag{21}$$

Where, the constant  $c_k = 0.22$ .

To achieve the integration of (18), we assume constant values of these coefficients, putting  $C_{\mu z} = C_{\mu s}$  and  $\sigma_k = \sigma_{ks}$ , and, in the expression of the production term,  $P_r = \frac{\varepsilon}{C_{\mu z} k^2} (\overline{-uw})^2$ , we only retain the principal contribution when  $\xi \rightarrow 1$ , that is, with (19) and (20):

$$P_r \approx \frac{\gamma u^{*4} (1 - \xi)^2}{C_{\mu z} L_s k_s^{0.5}} \tag{22}$$

With this set of assumptions, equation (18) may be rearranged as: 
$$\frac{\partial^2}{\partial \xi^2} k^{+3/2} = \frac{1}{l_s^{+2}} k^{+3/2} - P_r^+ \tag{23}$$

$$\text{where: } k^+ = k/u^{*2}, \quad L_s^+ = \frac{L_s}{h}, \quad l_s^+ = \sqrt{\frac{2 C_{\mu s}}{3 \sigma_{ks}}} L_s^+ \quad \text{and} \quad P_r^+ \approx \frac{\gamma(1-\xi)^2}{C_{\mu s} l_s^{+2} k_s^{+0.5}} \quad (24)$$

$$\text{We integrate (23) with the boundary conditions: } \xi = 1, k^+ = k_s^+ \text{ and } \frac{\partial k^+}{\partial \xi} = 0 \quad (25)$$

Finally the fields of turbulent kinetic energy and turbulent dissipation rate may be expressed as:

$$k^+ = \frac{k}{u^{*2}} = k_s^+ [(1-\alpha) \cosh\left(\frac{1-\xi}{l_s^+}\right) + \alpha \left(1 + \frac{1}{2} \left(\frac{1-\xi}{l_s^+}\right)^2\right)^{2/3}] \quad \text{and} \quad \alpha = \frac{2\gamma l_s^{+2}}{C_{\mu s} k_s^{+7/2}} \quad (26)$$

$$\varepsilon^+ = \frac{\varepsilon h}{u^{*3}} = \frac{k^{+3/2}}{l_s^+} = \frac{k_s^{+3/2}}{l_s^+} \left[ ch\left(\frac{1-\xi}{L_s^+}\right) - 2\beta sh^2\left(\frac{1-\xi}{2L_s^+}\right) + \frac{\beta}{2} \left(\frac{1-\xi}{L_s^+}\right)^2 \right] \quad (27)$$

### 3. Application to the experimental results

These asymptotic solutions were applied to the results of an experience achieved in a rectangular open channel, (fig. 3). The channel is 0.52 m wide, 0.2 m deep and 13.5 m long and the bed slope was adjusted to 0.20%. The roughness is made up with rectangular PVC plates, 5 mm thick and 3 cm wide, periodically glued in the central zone of the channel bottom, on the third of the width; the other part of the bottom is smooth as well as the lateral walls. In Run Za, the water depth, measured from the top of roughness, was  $h = 0.078$  m, and the flow rate  $Q = 22$  l/s.

A two component laser Doppler anemometer (LDA-2D) is used to carry out velocity measurements at a section situated 9.5 m downstream from the entrance, where the flow was fully developed. We measured in the half section of the channel the mean longitudinal and vertical velocity  $U$  and  $W$ , the turbulent shear stress  $-\overline{uw}$ , the longitudinal and normal fluctuations  $\overline{u^2}$  and  $\overline{w^2}$ , following 25 transverse verticals. Detailed information on experimental techniques and results could be found in [4, 13, 14].

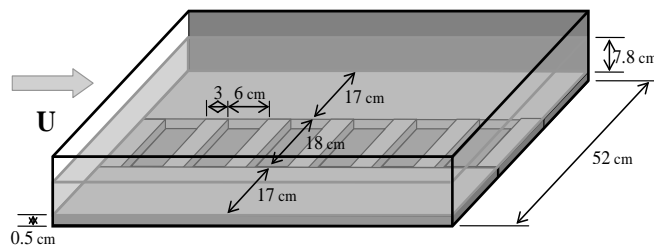


Fig. 3. The open channel with the transverse variation of bottom roughness

The influence of the secondary motions (fig.4) on the vertical profiles of the Reynolds tensor component is presented on fig. (5) where non-dimensional turbulent shear stress profiles of  $-\overline{uw}/u^{*2}$  are plotted versus the external variable  $\xi$ . We note an important decrease of  $-\overline{uw}/u^{*2}$  near the wall, in the zone of roughness change ( $y=9$ cm). This diminution is linked to the downward secondary flow orientation in that region (see fig.4). In the section  $y=16$ cm, the deviation from the linear distribution  $-\overline{uw}/u^{*2} = 1 - \xi$ , obtained in parallel flow, is related to the transport of longitudinal momentum by the ascendant secondary flows in this region (fig.4).

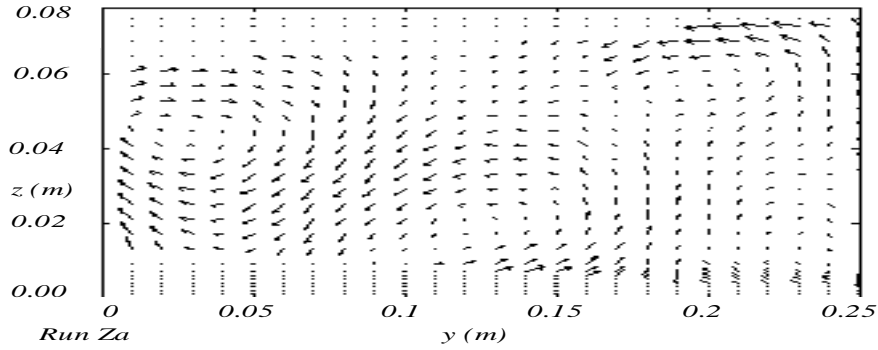


Fig. 4. Secondary flow structure in a half section of the channel

On figures 6 and 7 are plotted the vertical profiles of the normal Reynolds tensor components versus the external variable. Curves named (Mod) represent the asymptotic solutions, near the wall and near the free surface (see table 1). This analysis shows that the decrease of the turbulent intensity  $\overline{u^2}/u^{*2}$  and  $\overline{w^2}/u^{*2}$  in the wall region above the rough bottom, where the levels do not exceed, respectively, 4.5 and 1.1 (see fig. 6), and in particular in the zone of the roughness change at the section  $y=9\text{cm}$ , is directly related to the secondary flows effect (fig 4) on the turbulent shear stress which controls the turbulent kinetic energy production. We note in particular that this turbulence production diminution is due to the turbulent shear stress decrease in the wall region ( $\alpha = 2$  in fig 5).

In a similar way, we note that the increase of the turbulent intensity  $\overline{u^2}/u^{*2}$  and  $\overline{w^2}/u^{*2}$  in the wall region above the smooth bottom, where the levels become superior, respectively, to the values 4.5 and 1.1 (see fig. 7), and in particular at the section  $y=16\text{cm}$ , is also directly related to increase of turbulence production, due to the turbulent shear stress increase, in this region ( $\alpha = 0.4$  in fig 5).

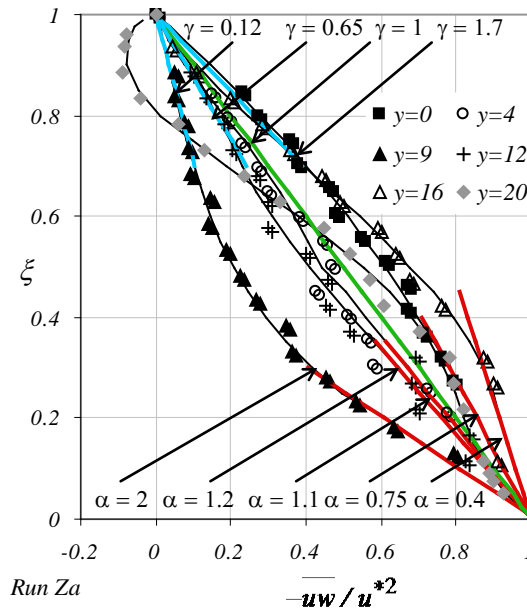


Fig. 5. Dimensionless turbulent shear stress

In the sections  $y=4\text{ cm}$  and  $y=12\text{ cm}$ , where the vertical profiles of  $-\overline{uw}/u^{*2}$  are quasi-linear, the wall laws of the one dimensional flow (1D vertical) are verified (see fig. 6 and 7). On these figures we also included flow measurements of [16] above smooth wall, these agreed with measurements in sections  $y=4$  and  $12\text{cm}$ , where the

vertical profile of  $-\overline{uw}/u^{*2}$  are quasi-linear.

Table 1. Values of the constant A and the free surface parameters

Wall region			
Section	Calculation	Constant A	$\alpha$
y=0 cm	Mod 0	0.75	0.75
y=4 cm	Mod 4	0.75	1.1
y=9 cm	Mod 9	0.75	2.0
y=12 cm	Mod 12	0.6	1.2
y=16 cm	Mod 16	0.6	0.4
y=20 cm	Mod 20	0.6	Smoothing
Free surface region $\xi > 0.6$			
Calculation	$K_s^+$	$L_s/h$	$\gamma$
Mod 0	1.6	1.35	1.7
Mod 4	1.7	1.7	1.0
Mod 9	1.2	1.85	0.12
Mod 12	1.8	1.9	0.65
Mod 16	1.6	1.15	1.7
Mod 20	1.9	1.6	Smoothing

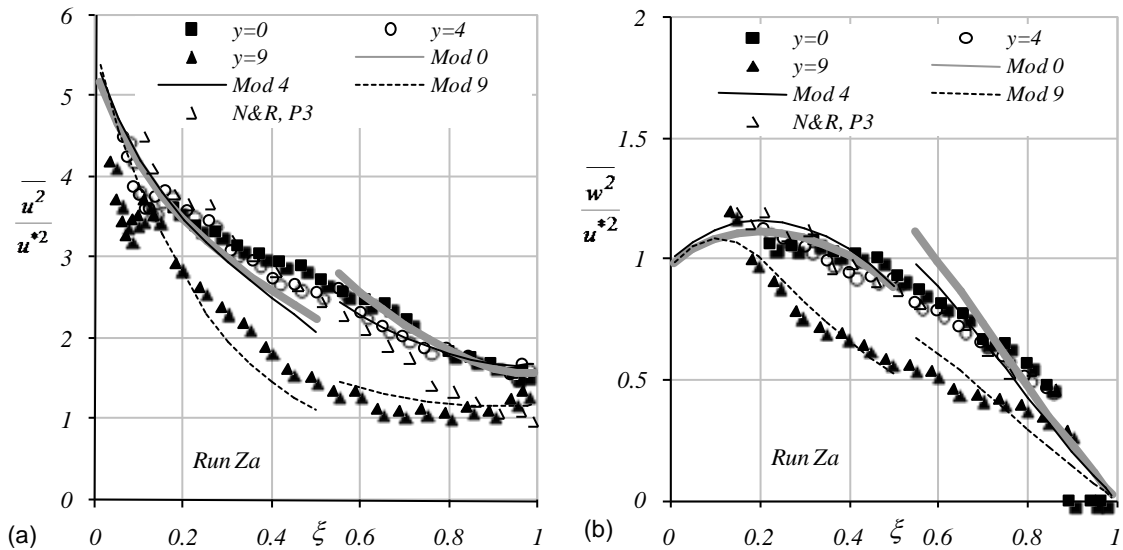


Fig. 6. Profiles over the rough zone: (a) Longitudinal fluctuation; (b) Vertical fluctuation

We also show on figures 6 and 7 that there is a good agreement between the experimental results and the analytical solutions developed to predict the turbulence intensity and the anisotropy in the wall and free surface region. Near the wall, the model restitutes the effect of secondary flows on the turbulence intensity via the decrease of the turbulence production due to the important decrease of the shear stress in the zone of roughness change at the section y=9cm. The model predicts also relatively well the increase of the normal velocity fluctuations near the wall at the section y=16. It gives good estimations of the turbulence intensity, by means of the adjustment of the turbulent diffusivity parameter  $C_{\mu}$ , through the constant A. This constant controls the vertical gradient of the mean velocity in the wall region, and consequently the production of turbulence. Near the free surface the asymptotic solution gives a good prediction of the longitudinal and vertical fluctuations when the effects of secondary flows are weak as in the sections y=16.

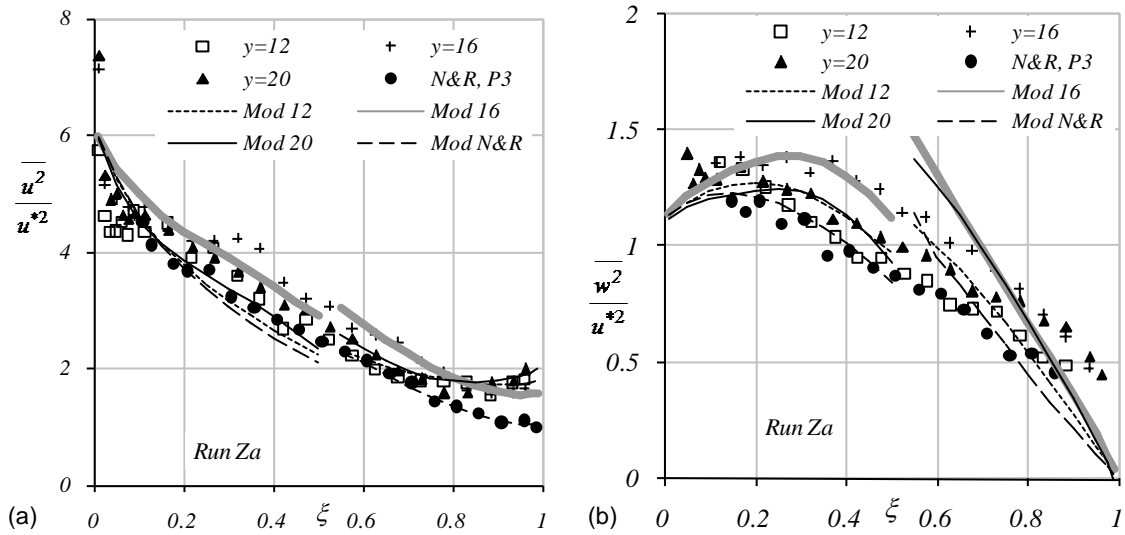


Fig. 7. Profiles over the smooth zone: (a) Longitudinal fluctuation; (b) Vertical fluctuation

Fig. 8a-8b illustrate the turbulent kinetic energy redistribution between the normal Reynolds tensor components  $\overline{u^2}$  and  $\overline{w^2}$ .

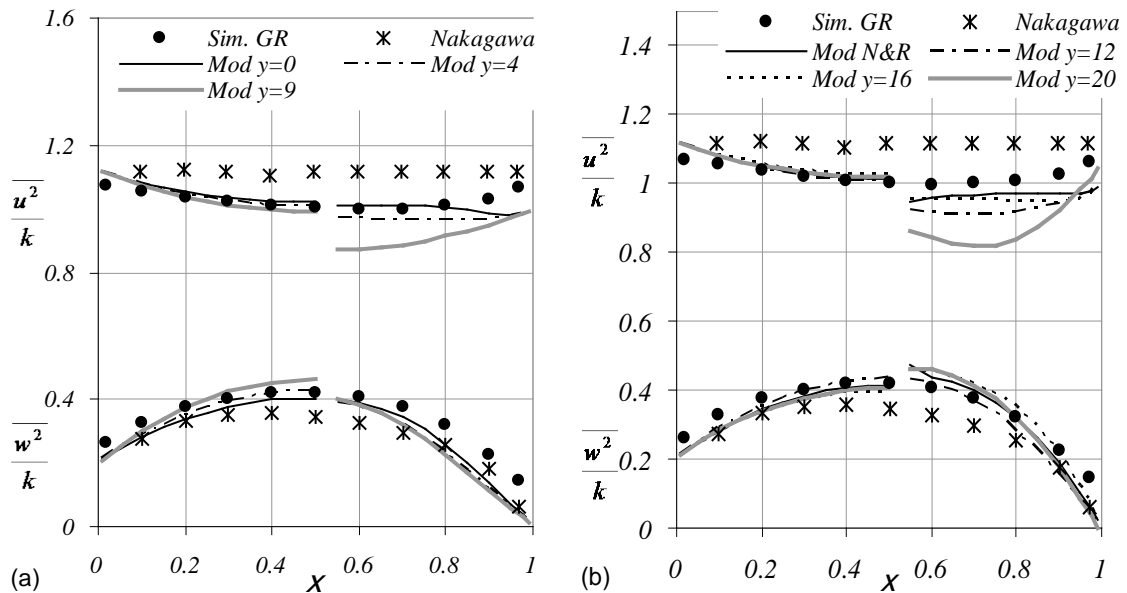


Fig. 8. Contribution of longitudinal and vertical turbulent stresses to the turbulent kinetic energy

On this figure the calculated profiles of  $\overline{u^2}/k$  and  $\overline{w^2}/k$  by the asymptotic solutions are compared to the numerical simulation (Sim GR) of [1] and also to the experimental results of [17]. First, we observe that all the calculations, in the vicinity of the wall, reaches the standard values  $\overline{u^2}/k \approx 1.1$  and  $\overline{w^2}/k \approx 0.25$ . We also note that the calculation (Mod  $y=0$ ) reproduces better the simulations of [1]. Second, we can see that in the wall region ( $\xi < 0.5$ ) the calculation values of  $\overline{u^2}/k$  are not very different, while values of  $\overline{w^2}/k$  are more different. This

indicates that, in these calculations, the turbulent kinetic energy redistribution between the lateral and vertical fluctuations is different, and consequently leads to differences in the level of anisotropy ( $\overline{v^2} - \overline{w^2}$ ).

Near the free surface, the comparison between different simulations of  $\overline{u^2}/k$  and  $\overline{w^2}/k$  is more delicate to interpret, because the analytic solution does not take into account of the advective transport by secondary flows.

#### 4. Conclusions

An inhomogeneous distribution of turbulent properties in the cross-stream section of a free surface flows, has been generated by roughness contrast induced on the wall bottom. In such situations, the wall laws formulation must take into account the effects of roughness variations and momentum transport by secondary flows. For this reason, we have developed an asymptotic formulation of a Reynolds stress model valid in the equilibrium zone as well as in the vicinity of the free surface. The secondary flows, and roughness contrast effects on the turbulent stresses in the wall zone, are introduced in the expressions of the turbulent shear stresses and in the pressure-strain term respectively. This model formulation has guided us to determine the cross-stream evolution of the wall parameters. And we note the following conclusions relative to the turbulence in free surface flows with a roughness contrast on the bottom wall:

- The roughness configuration used in this study has generated a significant evolution of mean velocity and turbulent stresses in the cross-stream section. This evolution is clearly observed above the roughness zone and accentuated at the change roughness zone.
- The asymptotic formulation of the model support a realistic interpretation of our experimental data and permits to examine the double effect of cross-stream variations of the bottom roughness and secondary flows, on the turbulence in the wall region.

#### References

- [1] M. Gibson and W. Rodi. "Simulation of free surface effects on turbulence with a Reynolds stress model." *Journal of Hydraulic Research*, 27(2), pp. 233-244, 1989.
- [2] I. Nezu and H. Nakagawa. "Turbulence in open channel flows." *IAHR-monograph* Balkema, 1993.
- [3] B. E. Launder and S. P. Li. "On the elimination of wall-topography parameters from second-moment closure." *Physics of Fluids*, 6(2) 999-1006, 1994.
- [4] S. Zaouali, A. Soualmia, L. Masbernat and C. Labiod. "Experimental determination of wall parameters of fully developed flow in an open channel with a sharp transverse bottom roughness," in *Proc. 11th Int. Mechanical Congress Agadir Morocco*, 2013.
- [5] C. Labiod, A. Soualmia and L. Masbernat. "Turbulence in open channel flow with a cross-stream variation of the bottom roughness," in *Proc. ISEH-V Arizona State University USA*, 2007, pp. 56-62.
- [6] J. O. Hinze. "Experimental investigation on secondary currents in the turbulent flow through a straight conduit." *Applied Scientific Research*, 28, pp. 453-465, 1973.
- [7] A. Soualmia. "Structure et modélisation des systèmes de fluides industriels et environnementaux." *Habilitation Universitaire*, E.N.I.Tunis, pp. 87, 2008.
- [8] S.J. McLelland, P. J. Ashworth, J.L. Best and J.R. Livesey. "Turbulence and secondary flow over sediment stripes in weakly bimodal bed material." *Journal of Hydraulic Engineering*, ASCE, 125(5), pp. 463-473, 1999.

- [9] Z. Q. Wang, N. S. Cheng, Y. M. Chiew and X. W. Chen. "Secondary flows in open channel with smooth and rough bed strips." *In Proc. XXX IAHR Congress Greece*, 1, 2003, pp. 11-118.
- [10] Z. Q. Wang and N. S. Cheng. "Secondary flows over artificial bed strips." *Advances in Water resources*, Vol. 28, Issue 5, pp. 441-450, 2005.
- [11] Z. Q. Wang and N. S. Cheng. "Time-mean structure of secondary flows in open channel with longitudinal bed forms." *Advances in Water resources*, Vol. 29, Issue 11, pp. 1634-1649, 2006.
- [12] J. F. Rodriguez and M. F. Garcia. "Laboratory measurements of 3-D flow patterns and turbulence in straight open channel with rough bed." *Journal of Hydraulic Research*, vol. 46, No. 4, pp. 454-465, 2008.
- [13] S. Zaouali. "Structure et modélisation d'écoulements à surface libre dans des canaux de rugosité inhomogène." M.A. Thesis, I.N.P.Toulouse/E.N.I.Tunis, pp. 163, 2008.
- [14] S. Zaouali, A. Soualmia, L. Masbernat and C. Labiod. "Experiments on Turbulence in open channel flow on rough bottom wall." *in Proc. Second International Symposium on Shallow flow* Hong Kong, 2008, A0114.
- [15] M. M. Gibson and B. E. Launder. "Ground effects on pressure fluctuations in the atmospheric boundary layer." *Journal of Fluid Mechanics*, 86, pp. 491-511, 1978.
- [16] I. Nezu and W. Rodi. "Open-channel flow measurements with a laser Doppler anemometer." *Journal of Hydraulic Engineering*, 112(5), pp. 335-355, 1986.
- [17] H. Nakagawa, I. Nezu and H. Ueda. "Turbulence of open channel flow over smooth and rough beds." *in Proc. Of JSCE*, 241, 1975, pp.155-168.